Desalination and Water Treatment
www.deswater.com
doi: 10.5004/dwt.2021.26596

210 (2021) 31–43
January

Numerical studies on the heat transfer characteristics of falling film evaporation on a horizontal elliptical tube for seawater desalination

D. Balaji[a,*], R. Velraj[b], M.V. Ramana Murthy[a]

[a]*Department of Ocean Structures, National Institute of Ocean Technology, NIOT Campus, Velachery-Tambaram Main Road, Pallikaranai, Chennai-600100, Tamil Nadu, India, Tel. +91-044-6678 3349; Fax: +91 044 6678 3580; email: dbalaji@niot.res.in (D. Balaji), Tel. +91-044-6678 3586; Fax: +91 044 6678 3580; email: mvr@niot.res.in (M.V. Ramana Murthy)*
[b]*Institute for energy studies, College of Engineering, Anna University, Sardar Patel Road, Guindy, Chennai-600025, Tamil Nadu, India, Tel. +91-24562344; email: velrajr@gmail.com*

Received 18 February 2020; Accepted 17 September 2020

ABSTRACT

This paper discusses the effect of elliptical tube geometry on the heat transfer performance of falling film evaporation over the horizontal heated plain tubes in comparison with circular tubes for seawater desalination. To study this, a two-dimensional CFD model was developed, compared and validated with published data available in the literature. A CFD simulation was carried out for varying liquid load, ellipticity (*E*) and corresponding changes in the film heat transfer co-efficient (HTC), liquid film thickness were recorded and analysed. Also novelty in finding the commencement of the fully developed thermal region over the tube from current simulation model is discussed. An attempt was also made to measure the thickness of the film around the tubes from the CFD model. Mechanisms that influences enhancement in heat transfer using the elliptical tubes were numerically investigated and discussed in the present work. Outputs from simulation model indicated that low value of liquid film thickness appears approximately at the angular position of the range between 90° and 110°. Also this study revealed that liquid film thickness decreases and HTC increases with the increase of ellipticity of the tube. Commencement angle of fully developed thermal region from top of tube shifted downward with the increase of the liquid load. For the same operating conditions, the elliptical tube gives 24%–26% more HTC and 8%–18% thinner film thickness compared with the circular tubes indicating better suitability of elliptical tubes for seawater desalination.

Keywords: Elliptical tubes; Ellipticity; Film heat transfer co-efficient; Fully developed thermal region

1. Introduction

Falling film evaporation with horizontal tubes finds its application in multi-effect desalination (MED) plants, refrigeration and food processing industries, chemical processing industries, etc. [1]. Falling film evaporator generally operates with small temperature difference [2]. Even though it has wide range of applications, mechanism responsible for the heat transfer between the adjacent tubes still needs deep investigation. Convective heat transfer and nucleate boiling are the two modes of heat transfer that usually takes place in this type of evaporator. Generally, three types of mode are observed in liquid film flow around the horizontal heated tubes such as drop mode, column mode and sheet mode. Among that sheet mode provides better heat transfer co-efficient (HTC) due to proper distribution of liquid film all around the tube walls [3].

At low heat fluxes, convective mode of heat transfer takes place that resulted in occurrence of evaporation at the liquid–vapour interface. HTC of film normally hikes up

* Corresponding author.

with liquid film load until a particular film thickness reaches above which co-efficient value experiences no further improvement due to the development of thermal resistance [4]. Tahir et al. [5] discussed about the major challenges involved in the falling film evaporators used in MED plant such as attaining uniform liquid load over the tube bundle to avoid dry patches and scale formation. Their studies focussed on critically analysing the CFD works related to falling film evaporator for MED plants. They presented the CFD modelling and methodologies followed by identification of key research gaps based on the hydrodynamics and heat/mass transfer aspects of falling film evaporators.

Mal-distribution of the liquid spray over the tubes and dry out conditions are some of the drawbacks noticed in the falling film evaporation in horizontal tube bundles. Non-uniformity in flow distribution happens in the deeper portion of the tube bundle along the tube length as the flow of liquid moves under gravity. This hinders the heat transfer performance of the falling film evaporation. Most of the experimental study highlights that nucleate boiling takes place at high heat fluxes, with no marked influence of the film flow on the HTC. Increased heat flux at low liquid film flow resulted in the formation of the dry surfaces on the tube surface due to the Marangoni effect that retards the performance of falling film evaporation [6].

Above-mentioned issues are generally observed in the horizontal tube falling film evaporation of especially circular tubes. In order to minimise these issues and enhance the heat transfer rate, studies related to various tube shapes have been carried out by few researchers for improving the heat transfer performance of falling film evaporation. One such shape used in the present study is elliptical shape. They are generally identified by the ellipticity or shape factor (E). In this perspective, some of the studies related to elliptical tube available in the literature and appropriate for the present numerical study are discussed here. Luo et al. [7] presented a two-dimensional CFD study of the horizontal tubes falling film evaporation using different shapes for seawater desalination application. The shape includes one circular tube, non-circular shaped tubes, a drop-shaped tube and an oval-shaped tube. The volume of fluid (VOF) model was used to determine the effect of liquid film flow and feeder height on the film distribution thickness and heat transfer performance. Numerical results indicated that minimum thickness observed at angular positions of 125°, 160° and 170° for smooth circular, oval and drop-shaped tubes, respectively. Increase of film thickness with increase of film flow and decrease of feeder height is observed. Drop and oval-shaped shows better performance compared with circular shape due to formation of thinner thermal boundary layer.

Hasan and Siren [8] conducted experimental study on the elliptical as well as circular tubes and observed that elliptical tubes exhibit 1.93–1.96 times heat transfer rate compared with the circular tubes. Chen and Chen [9] carried out boiling heat transfer experiments on the perforated horizontal tube falling film evaporator using elliptical tubes. This study proves that perforation on the ellipticity of the tube significantly improves the heat transfer rate of the evaporator. Javad and Mahnaz [10] followed a numerical approach for investigating the effect of ellipticity of the ellipse, Brinkman numbers, and Reynolds number on the irreversibility for analyzing the entropy generation in a forced convection film condensation on a horizontal isothermal elliptical tube. It is observed from the result that ellipticity found to be having a significant effect on the total entropy generation number when E (ellipticity) > 0.7. Qi et al. [11] conducted numerical studies, experiments and method of theoretical analysis on the falling film liquid flow and heat transfer on circular shaped tube and elliptical tube. They noted a better heat transfer improvement in these tubes compared with round-shaped tubes. They showed that the liquid film thickness of elliptical tube from the simulation matches well with the experimental data. Maximum deviation between the results was within 8%. The experimental results also indicated that HTC of elliptical tubes increases by 20%–22% when compared with circular tubes. This study proved and paved a way for application of falling film evaporation with elliptical tubes in the seawater desalination system.

Sideman et al. [12] carried out an analysis of simultaneous condensation inside and evaporation outside a horizontal conduit for different shapes of conduits. The objective of the study is to improve the performance of horizontal evaporator–condenser water desalination units by finding the most promising shape. They observed that vertically oriented elongated elliptical conduits yield the highest overall HTCs among the shapes tested for different conduits. The effects of intermittent removal of the condensate film by internal horizontal films decreases as the major to minor axis ratio increases.

Lee et al. [13] conducted numerical studies on the evaporation heat transfer characteristics of obliquely dispensed falling films over a horizontal elliptical tube and validated the numerical studies with the data available in the literature. They applied VOF method to simulate the spreading development of falling liquid films for resolving the distribution of velocity, temperature, volume fraction in conjunction with the convective HTC. They developed user-defined function (UDF) for studying the evaporative effect at the liquid film and vapour interface. In this study, the HTC and liquid film distribution around the circular and elliptical tube surfaces are determined and compared with the experimental results available in the literature and validated. They tested different flow models, in that SST k-ω model provides better accuracy and less calculation time compared with the other flow models. It is observed that at a low liquid film flow rate of 0.093 kg/(m s), the liquid film was unable to fully cover the tube surface with the formation of dry areas, resulting in the significant drop in heat transfer effectiveness. Also achieved average HTC up to 4.18 kW/m^2 K at a high liquid flow rate of 0.186 kg/(m s) which indicates good thermal performance as observed in the literature reports. Also, it is noticed that reasonable average HTC can be attained for the variation of dispensed angle with in 30°.

Lee et al. [14] carried out CFD studies in which the influence of counter current airflow on evaporative heat transfer performance of falling film on a horizontal elliptical tube. The numerical analysis is based on the VOF model for catching the dispersal evolution of descending films in conjunction with the UDF to model the evaporation

effect at the water–vapour interface. A good agreement is observed between the computational model and measured data from literature. Calculations are done to elaborate the interaction mechanism of counter current air flows with the formation process and heat transfer of evaporative liquid films on the tubes. It is noted that upward air streams can induce the shear stresses at the liquid–air interface to form thicker wavy films. It is noted that counter current air flow enhances heat transfer in the lower part of the tube than the upper part. CFD studies are also carried out by varying the liquid flow rate of 0.093–0.186 kg/(m s) and counter airflow velocity of 0–3 m/s, respectively. A steeper temperature gradients is observed at the wall to enhance the heat transfer achieving an averaged HTC of 4.15 kW/m² K for Γ = 0.149 kg/(m s) and V_{air} = 3 m/s.

Pu et al. [15] carried out 2D CFD studies on a horizontal tube falling film evaporator using a circular tube and three flat tubes. In their work, they simulated the heat and mass transfer process and validated the predicted HTC with the experimental data. It is observed from this study that as the height–width ratio of the tube increases, the liquid film becomes thinner. Also noted, the average film thickness of three flat tubes is smaller by 2.9%–16.5% compared with the circular tube. The average HTC of three flat tube is higher than the circular tube by 2.2%, 4.2% and 11.2%, respectively.

The present study focuses on the numerical investigation on the influence of elliptical tube geometry and its ellipticity on the heat transfer characteristics of horizontal tube falling film evaporation in comparison with circular tube using CFD tool with published experimental data of Qi et al. [11] for seawater desalination. Qi et al. [11] carried out numerical study to evaluate the film thickness for circular and elliptical tubes. They compared their results with experimental data of their own work and validated. In the present work, the CFD analyses have been carried out for elliptical as well as circular tubes using input data of Qi et al. [11] and compared and validated the results with Qi et al. [11] and found a reasonable agreement which is discussed in the present study. According to the study by Chyu and Bergles [16], three different heat transfer regions are identified in the horizontal tube falling film evaporation. The top region of the tube is the jet impingement region, HTC is relatively high in this region due to liquid feed on the top of the tube at certain velocity. In the thermal developing region, no evaporation takes place but the liquid film is superheated to a fully developed region with heat from the tube is fully utilized for converting the saturated liquid into superheated liquid. In the fully developed thermal region, the superheated liquid started evaporating due to convective heat transfer at the liquid–vapour interface, provided no nucleate boiling is observed within the film. The novelty in predicting the commencement of the fully developed thermal region from the present simulation model well matches with the findings of Chyu and Bergles [16].

2. Problem statement

In order to investigate the present study using CFD, two physical models are developed. One of physical model is of elliptical shape of ellipticity, E = 1.5 as shown in Fig. 1 and other one is of circular tube of 25 mm outer diameter as shown in Fig. 2. Working pressure maintained in the CFD studies for these models is 312 mbar. Wall temperature of tube maintained at 71.2°C and feed water at 69.8°C. Saturation temperature in the external portion of the tubes kept at 70°C. The spray density load for this model varies between 0.02 and 0.06 kg/(m s). The maximum Reynolds number in the analysis reaches up to 1,750.

These models simulate the falling film evaporation of MED process. The steam that passes inside the tube condenses and also transfers heat in the form of latent heat condensation to the liquid film flowing outside tubes. The feed liquid spray density over the tube is indicated by 2Γ, where Γ (kg/(m s)) is the liquid feed rate per side and per unit length of the tube. Sea water is used as feed water in the present analysis. In the analysis, properties of the seawater are carefully selected for density and viscosity. Ansys Fluent 14.0 version is used for the present analysis.

The assumptions given below are adopted from the study by Balaji et al. [17] for the CFD analysis:

- Film flow is assumed to be laminar.
- Sheet mode of liquid film is assumed in this study.
- Gravity force is considered dominant than the inertial force.
- Evaporation occurs only at the liquid–vapour interface.
- No occurrence of nucleate boiling in the liquid film.
- Scale formation on the tubes is negligible.
- Liquid density is assumed to be constant.

3. Governing equations and physical models

The following mathematical equations as adopted from the study by Balaji et al. [17] are described below for present simulation studies. The flow in the present simulation model

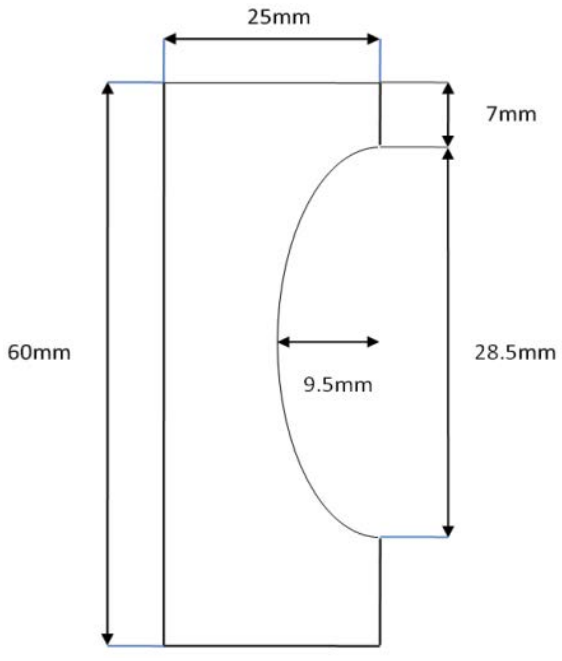

Fig. 1. Physical model of elliptical tube (E = 1.5).

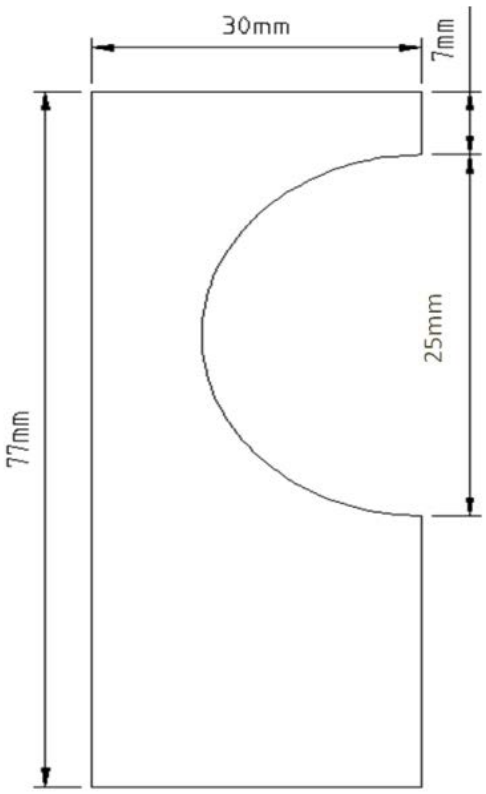

Fig. 2. Physical model of circular tube (25 mm OD).

is governed by the Navier–Stokes equation. The continuity equation is given as follows:

$$\frac{\partial \rho}{\partial t} + \nabla \cdot (\rho v) = 0 \tag{1}$$

The momentum equation in horizontal direction (x-axis) is given by:

$$\frac{\partial u}{\partial t} + u \cdot \frac{\partial u}{\partial x} + v \cdot \frac{\partial u}{\partial y} = -\frac{1}{\rho}\frac{\partial p}{\partial x} + v\left(\frac{\partial^2 u}{\partial x^2} + \frac{\partial^2 u}{\partial y^2}\right) \tag{2}$$

The momentum equation in vertical direction (y-axis) is given by:

$$\frac{\partial v}{\partial t} + u \cdot \frac{\partial v}{\partial x} + v \cdot \frac{\partial u}{\partial y} = -\frac{1}{\rho}\frac{\partial p}{\partial y} + g + v\left(\frac{\partial^2 v}{\partial x^2} + \frac{\partial^2 v}{\partial y^2}\right) \tag{3}$$

The fluid energy equation is given by:

$$\frac{\partial T_L}{\partial t} + u \cdot \frac{\partial T_L}{\partial x} + v \cdot \frac{\partial T_L}{\partial y} = \left[\alpha_L \frac{\partial^2 T_L}{\partial x^2}\right] + \left(\alpha_L \frac{\partial^2 T_L}{\partial y^2}\right) \tag{4}$$

3.1. Evaporation–condensation model

The evaporation–condensation model (liquid–vapour mass transfer) is governed by vapour transport equation as shown below [17,18]:

$$\frac{\partial}{\partial t}(\alpha \rho_v) + \nabla \cdot (\alpha \rho_v V_v) = m_{l \to v} - m_{v \to l} \tag{5}$$

where ρ is the density, T_L is the liquid temperature; u is the x-component of water velocity, v is the y-component of water velocity, α_L is the thermal diffusivity, g is acceleration due to gravity in y-direction, ν is vapour phase, α is vapour volume fraction, ρ_v is vapour density, V_v is the vapour phase velocity, $m_{l \to v}$ and $m_{v \to l}$ are the rate of mass transfer due to evaporation and condensation, respectively, (kg/m^3 s).

The $m_{l \to v}$ and $m_{v \to l}$ are determined using the following relations as given below [18]:

If $T_L > T_s$ then

$$m_{l \to v} = \text{coeff} \cdot \alpha_l \cdot \rho_l \cdot \frac{T_L - T_s}{T_s} \tag{6}$$

If $T_L < T_s$ then

$$m_{v \to l} = \text{coeff} \cdot \alpha_v \cdot \rho_v \cdot \frac{T_v - T_s}{T_s} \tag{7}$$

where coeff is co-efficient of mass transfer determined by the following equation [19]:

$$\text{coeff} = \frac{\text{Cp}_l \cdot T_s}{L_v} \tag{8}$$

where L_v is the latent heat of evaporation (kJ/kg) and T_s is saturation temperature. Using Eq. (8) the mass transfer co-efficient can be determined. Current analysis involves evaporation of liquid at the interface. Coeff in Eq. (8) denotes the mass transfer intensity factor or relaxation time with unit s^{-1}. The value of coeff is recommended to be such as to maintain the interfacial temperature reasonably close to the saturation temperature as well as to avoid divergence issues.

3.2. VOF model

VOF model is proposed by Hirt and Nichols [20] in 1981. Falling film evaporation is a complex phenomenon in nature. With the development in the computational field, it becomes feasible to study and analyse the different flow modes and their dynamic behaviour. According to Hirt and Nichols [20], capturing and tracking the liquid/vapour interface is one of the challenging task. They developed VOF model based on Eulerian approach for identifying, tracking and locating the liquid/vapour interface. They reconstructed the mass conservation equation for each phase using void fraction α [5]. According to Hirt and Nichols [20], the value of the volume fraction (α) lies between 0 and 1. The sum of the volume fractions of all phases is equal to 1 for each grid cell:

$$\alpha_l + \alpha_v = 1 \tag{9}$$

The governing equations of the volume fractions are given as follows:

$$\frac{\partial \alpha_l}{\partial t} + \nabla \cdot \left(\vec{v} \cdot \alpha_l\right) = \frac{\dot{m}_l}{\rho_l} \tag{10}$$

$$\frac{\partial \alpha_v}{\partial t} + \nabla \cdot (\vec{v} \cdot \alpha_v) = \frac{\dot{m}_v}{\rho_v} \tag{11}$$

where

$$\dot{m}_l = -\dot{m}_v \tag{12}$$

The momentum equation can be expressed as follows:

$$\frac{\partial \alpha_v}{\partial t}\left(\rho \vec{v}\right) + \nabla \cdot (\rho \vec{v}\vec{v}) = -\nabla_p + \nabla\left(\mu\left(\nabla \vec{v} + \nabla \vec{v}^T\right)\right) + \rho \vec{g} + F_V \tag{13}$$

where

$$\rho = \rho_l \cdot \alpha_l + \rho_v \cdot \alpha_v \tag{14}$$

$$\mu = \mu_l \cdot \alpha_l + \mu_v \cdot \alpha_v \tag{15}$$

where v represents the vapour phase and l represents the liquid phase. The fluid properties such as density (ρ) and viscosity (μ) for each phase are computed based on the volumetric change.

In order to include the surface tension effect in VOF model, Brackbill et al. [21] proposed a continuum surface force model in which surface force is converted into volume force, F_v, which can be expressed as follows:

$$F_v = \sigma \cdot K \cdot \nabla \alpha_l \cdot \frac{\rho}{\frac{1}{2} \cdot \left(\rho_l + \rho_v\right)} \tag{16}$$

where K represents the surface curvature. It is evaluated from the local gradients in the surface normal at liquid–vapour interface.

$$K = -\nabla \cdot n \tag{17}$$

The surface unit normal vector n at cell next to wall for specified contact angle θ_w is given below:

$$n = n_w \cdot \cos\theta_w + t_w \cdot \sin\theta_w \tag{18}$$

where n_w and t_w are normal and tangential unit vectors, respectively.

Ellipticity of the tube (E):

According to Qi et al. [11], the ellipticity of the elliptical tube is defined as follows:

$$E = \frac{a}{b} \tag{19}$$

where a = longer (vertical) axis of elliptical tube (a = 28.5 mm), b = minor axis of elliptical tube (b = 19 mm).

4. CFD modelling and analysis

In recent years, CFD is used commonly for investigating the two-phase heat transfer which is a cumbersome phenomenon as in the current work, where falling film evaporation of liquid happens over horizontal heated tubes in a low vacuum atmosphere. Two different 2D CFD models are developed based on the operating conditions followed by Qi et al. [11] in their experimental works for seawater desalination. Same operating parameters are given as input to the present CFD model. Physical domain of both the models developed based on the studies by Qi et al. [11]. Saturation pressure and temperature of around 312 mbar and 70°C are maintained, respectively, in the outside portion of the tubes. Outside wall temperature of tubes is kept at 71.2°C. Orifice size of inlet is 1.5 mm. GAMBIT software is used for modelling and meshing of these two domains. Considering the advantage of the symmetric shape, half of the domain is modelled for reducing the processing time. In the regions of the curved surfaces, the fine mesh is adopted to resolve flow physics without any complications. Half models in the meshed conditions for both the problems are shown in Figs. 3 and 4, respectively. In the pre-processor, the boundary conditions such as velocity inlet and pressure flow outlet are enabled then they are imported into the FLUENT for carrying out the simulation studies. This tool implements the method of finite volume for solving the energy conservation, mass and momentum equations. PISO algorithm is chosen as the solver option for the transient simulation with an under relaxation factor of 0.3 for pressure and 0.7 for momentum and Green Gauss cell-based gradient is chosen for the CFD analysis [17]. A fully implicit method and body force formulation is adopted for the present study. A first-order upwind differencing scheme is adopted in the present study. From the grid independence study, it is noted that no improvement in accuracy happens beyond meshes with 110,339 cells and also adds to the increment in the computational processing time. Size of each cell is around 0.03 mm. A time independence study is carried out by keeping time step at 0.001 s. The details of the parameters used in the fluent analysis are shown in Table 1. The results of the analysis are discussed in Results and discussion section in comparison with the published results [11] under the same operating conditions for validation. In order to compare the results of the elliptical tubes with circular tube, CFD analysis is also carried out on circular tube of 25 mm outer diameter. Same pave meshing scheme is used in this model with 1,22,250 quadrilateral cells at 0.03 mm size arrived after carrying out grid independent study with 0.001 s time step. The detail of the grid independence study carried out on elliptical tube and circular tube with respect to liquid film thickness is indicated in Tables 2 and 3, respectively. The results are discussed in Results and discussion section in comparison with published results [11] under same operating conditions for validation. Convergence criteria of 10^{-3} and 10^{-5} are used for mass, momentum and energy residuals, respectively [17].

5. Results and discussions

5.1. Effect of the elliptical tube on the HTC in comparison with circular tube

CFD studies are carried out for finding the HTC values and film thickness around the tubes of falling film evaporation for elliptical tube (E = 1.5) model in comparison with

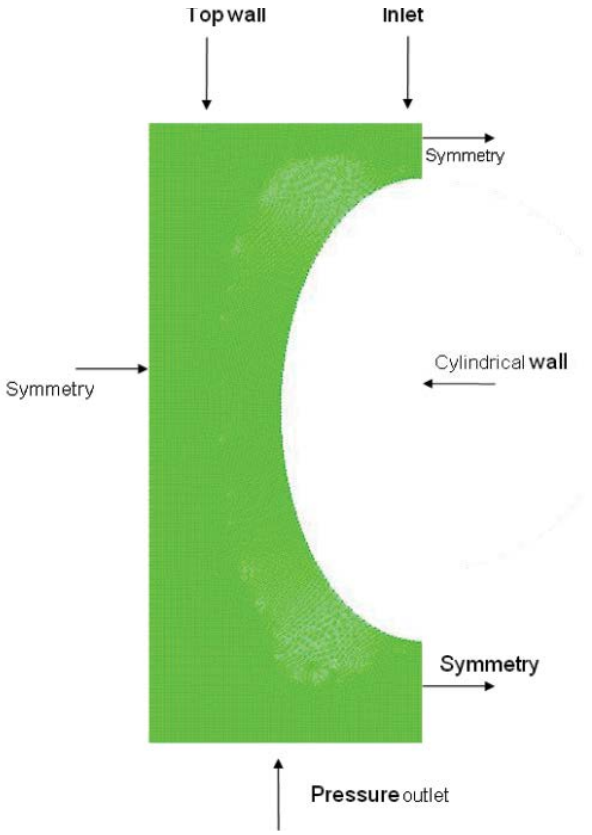

Fig. 3. Mesh model of elliptical tube.

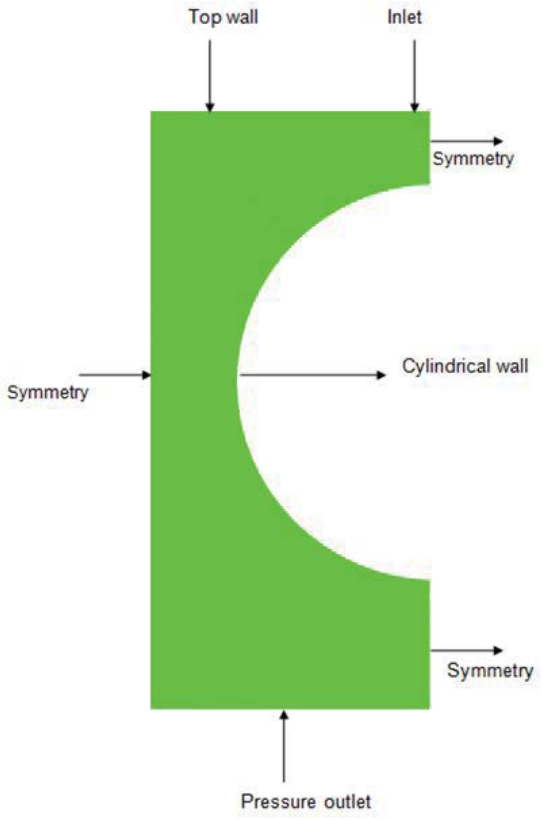

Fig. 4. Mesh model of circular tube.

25 mm OD circular tube for a given surface wall temperature and inlet conditions.

Input parameters of the present study are as follows:

- Inlet feed spray density load: 0.007 to 0.16 kg/(m s)
- Saturation pressure outside the tube surface: 312 mbar
- Saturation temperature: 70°C
- Tube wall temperature: 71.2°C
- Intake feed water temperature: 69.8°C

The tube wall temperature is maintained constant at 71.2°C throughout the analysis. The contours of HTC at wall region for spray density of (Γ) 0.05 kg/(m s) for the elliptical tube is indicated in Fig. 5a and for 25 mm diameter circular tube in Fig. 5b. Qi et al. [11] conducted experiments using elliptical tubes with E = 1.5 and compared the results with circular tube of 25 mm OD for different liquid spray density and measured the HTC of the falling film evaporation and liquid film thickness. In the present study, the CFD analysis is carried out using same operating parameters of the above work with the help of fluent software for validating the simulation model. In the analysis, the liquid spray density is varied between 0.04 and 0.14 kg/(m s) and corresponding changes observed in HTC are measured and recorded for comparative analysis in Fig. 6. The figure indicates the effect of spray density on the HTC for elliptical tube in comparison with circular tube. It is observed that the trend of the curve of the present CFD results is similar to the observations of Qi et al. [11]. A reasonable agreement of 10%–13% is observed between the results of the present CFD analysis and Qi et al. [11]. It is observed that increase of spray density resulted in the increase of the HTC values up to 0.09 kg/m s and after that horizontal pattern is observed for both elliptical and circular tubes for studies

Table 1
Details of parameters used in fluent analysis [17]

Simulation	2D
Solver	Pressure based, laminar, unsteady
Two-phase model	VOF
Primary phase	Air
Secondary phase	Water vapour and water
Gravitational acceleration	Downward direction in y
Tube wall	Constant temperature
Volume of fraction for water	1
Volume of fraction for vapour	0
Pressure velocity coupling	PISO
Discretization pressure	PRESTO
Discretization momentum	First-order upwind
Top boundary	Velocity inlet
Bottom side boundary	Pressure outlet
Side boundary	Symmetry
Wall boundary	Tube curvature

Table 2
Computational results of grid independence for 2D, Γ = 0.15 kg/(m s) for elliptical tube

Grid size (mm)	0.05	0.04	0.03	0.02
Liquid film thickness at θ = 90° angle (m)	0.000317	0.000314	0.000311	0.000311

Table 3
Computational results of grid independence for 2D, Γ = 0.15 kg/(m s) for circular tube

Grid size (mm)	0.05	0.04	0.03	0.02
Liquid film thickness at θ = 90° angle (m)	0.000369	0.000365	0.000363	0.000363

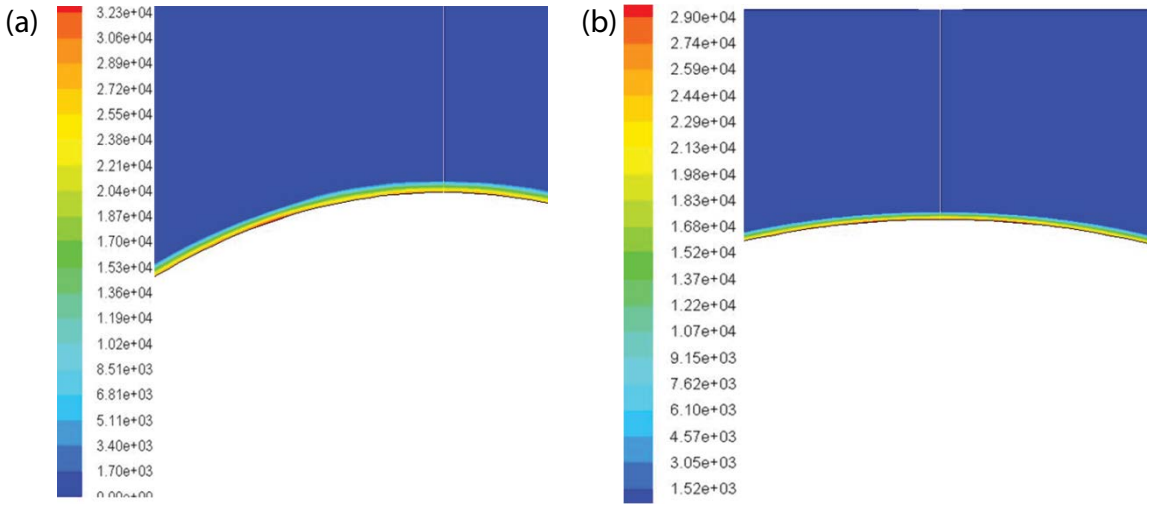

Fig. 5. Contours of heat transfer co-efficient (W/m² K) for spray density Γ = 0.05 kg/m s at T_{wall} = 71.2°C, and T_{sat} = 70°C for (a) elliptical tube (E = 1.5) and (b) circular tube (25 mm OD).

carried out by Qi et al. [11]. Whereas the present study predicted the HTC values that showed an increasing trend up to 0.12 kg/(m s) and maintains straight line after that. This could be due to the fact that thickness of the liquid film might be lesser than the results of Qi et al. [11] between the spray range 0.09 and 0.12 kg/(m s) which would certainly result in better conduction of heat with in the liquid due to less thermal resistance. A horizontal curve pattern observed as discussed above is due to the increased thermal resistance above certain flow rate where the liquid film thickens offers resistance against the heat transfer that resulted in no improvement in the HTC values. The deviation in results between the experimental and present numerical study could be due to the practical aspects that encountered in the experimental study carried out by Qi et al. [11] such as condensation of supplied steam inside the heating tube and resultant formation of condensate that influences the heat transfer rate and presence of dissolved gases in the evaporation space which are complex may influence the liquid film HTC. This phenomenon could not be considered in the present simulation study due to complexity.

It is observed from Fig. 7 that the results of Qi et al. [11] for both elliptical and circular tubes are varying by 20%–22% average, which means the HTC values of the elliptical tubes are higher than the circular tubes almost by 20%–22%. This is due to the fact that film thickness all around the elliptical tubes is dominated by the force of gravity better than that of the circular tube. This phenomena resulted in the reduced film thickness and increased film velocity in the elliptical tubes than the circular tubes which obviously develops better heat transfer rate and hence the co-efficient. The present CFD results also depicted that the HTC values of the elliptical tubes are found to be higher compared with the circular tubes with a percentage difference of 24%–26% average between elliptical and circular tubes.

It is also observed from Fig. 7 that HTC varies with circumferential angular position on the tube. At the stagnation region, that is, near to the 0° angle, highest HTC of 34.2 kW/m² K is observed and with further increment up to 15° angle, the HTC value slightly drops to reach the value of 33.8 kW/m² K called as impingement region. Velocity of liquid film in this region is higher next to the stagnation region; because of this, high HTC is observed here with better turbulence and decreased film thickness. After that, a sharp drop in HTC value is observed up to angle of around 56° angle and this region is called as thermally developing region. At the end of the thermally developing, the fully developed region commences. How to the identify the boundary between the thermally developed region and fully developed thermal region is discussed in Section 5.2

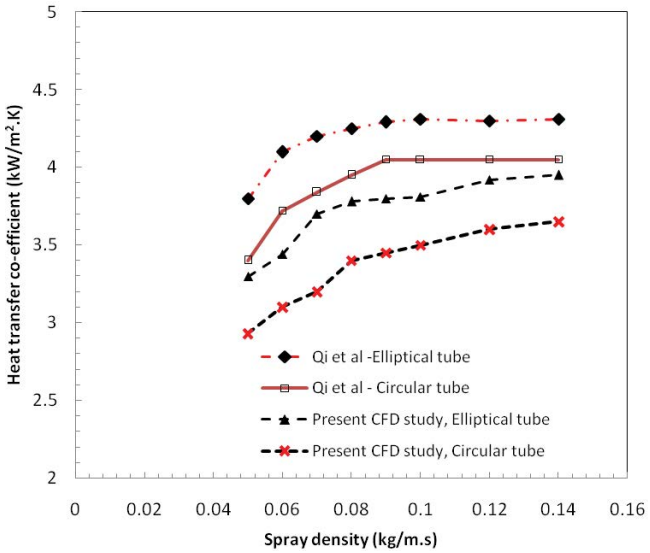

Fig. 6. Spray density (Γ) vs. heat transfer co-efficient (kW/m^2 K) at T_{wall} = 71.2 °C, and T_{sat} = 70°C for the elliptical tube and circular tube.

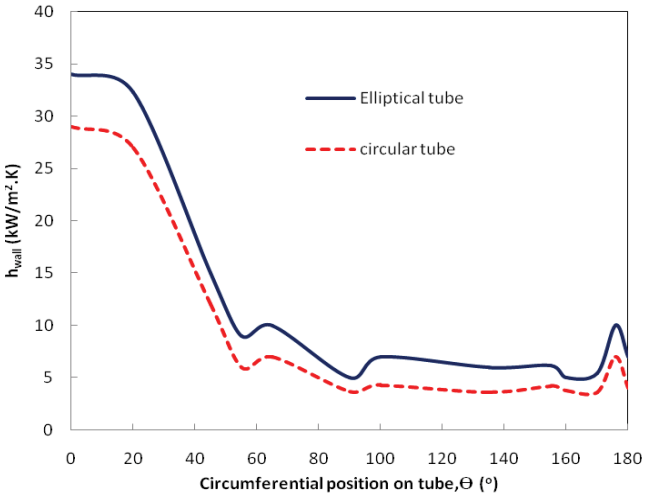

Fig. 7. Variation of HTC (kW/m^2 K) around the circumferential position of tubes for elliptical and circular tube at wall temperature T_{wall} = 71.2°C, Γ = 0.045 kg/m s, T_{sat} = 70°C.

and how the commencement of the fully developed region from the present numerical study perfectly matches with the theory suggested by Chyu and Bergles [16] based on their experimental study is also discussed in Section 5.6. It is also observed from Fig. 7 that the HTC values at any region of the elliptical tube is comparatively higher than the circular tube due to thinner liquid film on elliptical tube.

5.2. Studies on the effect of the elliptical tube on the commencement of fully developed region on the tubes for varying spray density in comparison with circular tube

Chyu and Bergles [16] indicated three different heat transfer regions as depicted in Fig. 8. The top region of the

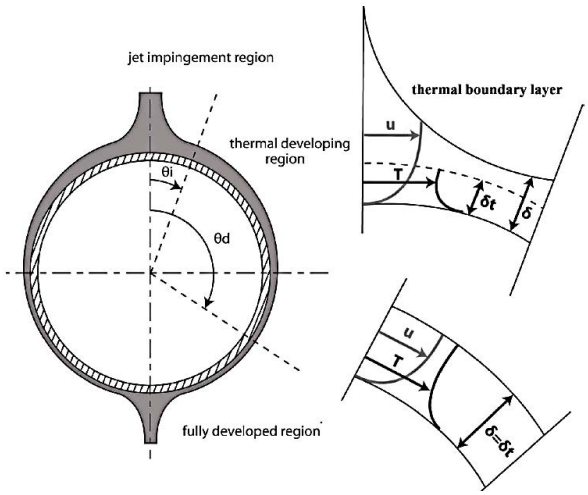

Fig. 8. Falling film thermal regimes [16].

tube is the jet impingement region, HTC is relatively high in this region due to liquid feed on the top of the tube at certain velocity. In the thermal developing region, no evaporation takes place but the liquid film is superheated to a fully developed region with heat from the tube is fully utilized for converting the saturated liquid into superheated liquid. In the fully developed thermal region, the superheated liquid started evaporating due to convective heat transfer at the liquid–vapour interface, provided no nucleate boiling is observed within the film.

In the present numerical study, the commencement of the fully developed thermal region is predicted using the contours of the mass transfer rate of the simulation model that exists in the region approximately between 20° and 70° angle, increases with an increase in the spray density which is indicated in Fig. 9 for both elliptical and circular tubes in comparison with mathematical model of Sharma et al. [22] of circular tube. The novelty of this prediction depends on the following factors such as [17]:

- Liquid film flow velocity
- Wall temperature of the tube
- Curvature length of the tube

Prediction of fully developed thermal region from the mass transfer rate contours of the simulation model is validated with the following references [17]:

- Studies conducted by Chyu and Bergles [16] on falling film evaporation which states that mass transfer rate or evaporation only occurs in the fully developed region and not anywhere else on the curvature of the tube.
- Mathematical model developed for the angular measurement of fully developed region by Sharma et al. [22].

The result of the present CFD study is compared with the work of the Chyu and Bergles [16]. According to them, the liquid film vaporization, that is, the mass transfer rate occurs in the fully developed thermal region and no sign of vapour formation is noticed in the thermally developing region until the fully developed region commences which

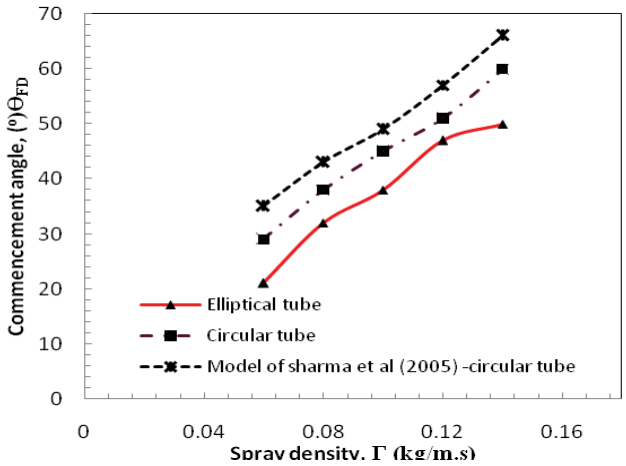

Fig. 9. Variation of commencement of fully developed region (θ_{FD}) (°) for elliptical and circular tube for varying spray density (Γ) at T_{wall} = 71.2°C and T_{sat} = 70°C.

is already discussed. It is observed from Figs. 10a–c that the mass transfer for this present CFD study occurs near to the 10° angle, 20° angle and 32° angle from the top of the tube corresponding to the feed rate of 0.04, 0.06, 0.08 kg/(m s), respectively, for elliptical tube where the fully developed thermal region commences according to the simulation which predicts no sign of evaporation before this region, that is, in the thermally developing region, which is in line with the findings of Chyu and Bergles [16]. Similar observation is also noted for the circular tube as indicated in Figs. 11a–c. To validate these models, the results of the CFD are compared with the mathematical model given in Eq. (20) developed by Sharma et al. [22] for the prediction of the fully developed thermal region (θ_{FD}) over circular tubes as given below.

$$\theta_{FD} = \pi - \left(\frac{1}{\pi \cdot \alpha \cdot R}\right) \cdot \left(\frac{3 \cdot \mu \cdot \Gamma^4}{g \cdot \rho^5}\right)^{\frac{1}{3}} \quad (20)$$

The percentage of the deviation between the mathematical model and CFD results are indicated in Table 4.

The effect of the spray density on the commencement of the fully developed region at a wall temperature of (T_{wall}) 71.2°C and saturation temperature of (T_{sat}) 70°C is indicated in Table 4 for both elliptical tube and circular tube. The CFD results are compared with the values obtained from the model developed by Sharma et al. [22] for circular tubes and validated. From the comparative study, it is observed that commencement angle of the circular tubes of CFD model is showing a reasonable agreement of 10% (average) with the output values of Sharma et al. [22] and 24% (average) agreement is found between Sharma et al. [22] model and elliptical tubes corresponding to the spray density that varies between 0.04 and 0.08 kg/m s. This high variation of 24% in elliptical tube is because of the model that is originally developed for the circular tubes by Sharma et al. [22]. It is also observed from Table 4 that the commencement angle of fully developed region of the elliptical tube from the top quadrant of the tube (i.e., 0° angle) is less or commenced earlier than the circular tube for the spray density range that varies between 0.04 and 0.08 kg/m s. This could be due to the fact that decreased film thickness and increased liquid film velocity on the elliptical tube surface compared with the circular tube resulted in better heat transfer that shrinks the thermally developing region where the temperature of the liquid film is increasing towards the saturation temperature by conduction of heat with in the liquid film and evaporation initiates once the liquid film bulk temperature reaches to or above saturation temperature corresponding to the surrounding pressure. It is also observed from Table 4 that with an increase of the spray density, the commencement angle of the fully developed region near to the tube surface increases. This could be due to the increased liquid film thickness, which resulted in the increased thermal resistance. This in turn lead to increased thermally developing region and reduced fully developed region, which is clearly observed in the contours of the mass transfer rate from Figs. 10a–c for elliptical tubes corresponding to varying spray density. Similarly, the contours of the mass transfer rate for circular tubes are indicated in Figs. 11a–c. From these figures, it is observed that increase of the liquid load resulted in the increase of the thermally developing region and decrease of the fully developed region, that is, increase of the commencement angle or delayed commencing of the fully developing region. It should be also

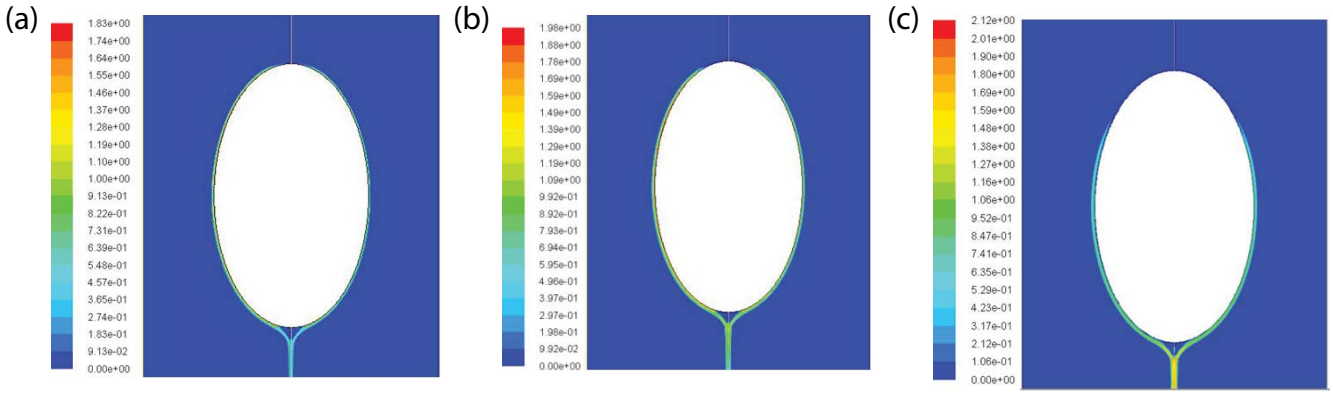

Fig. 10. Contours of mass transfer rate (kg/m^3 s) on elliptical tube for different spray density Γ (a) Γ = 0.04 kg/m s, (b) Γ = 0.06 kg/m s, and (c) Γ =0.08 kg/m s.

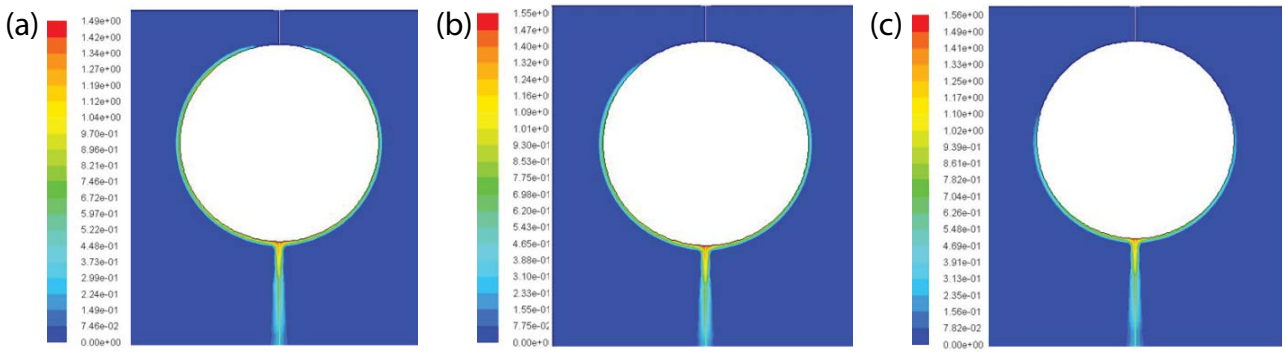

Fig. 11. Contours of mass transfer rate (kg/m^3 s) on circular tubes for different spray density Γ (a) Γ = 0.04 kg/m s, (b) Γ = 0.06 kg/m s, and (c) Γ = 0.08 kg/m s..

Table 4
Comparison of CFD results with mathematical model for fully developed commencement angle from 0° angle

	Present CFD results		Sharma et al. [22] model	
Spray density kg/(m s)	Elliptical tube	Circular tube	Circular tube	
	θ°_{fd}	θ°_{fd}	θ°_{fd}	Avg % deviation
0.04	10	14	15.5	9.6
0.06	20	28	31	9.5
0.08	32	36	40	10.1

noted that for the same spray density or liquid load, the curvature of tube under fully developed region is greater for the elliptical tube than the circular tube. This phenomenon attributed to possibility of high evaporation rate for the elliptical tube than the circular tube as the fully developed region is region where the evaporation actually takes place.

5.3. Effect of elliptical tube on the liquid film thickness for varying spray density in comparison with circular tube

The contours of the volume fraction of elliptical tube is shown in Figs. 12a–c corresponding to the liquid spray density (Γ) of 0.04, 0.06 and 0.08 kg/(m s), respectively. Similarly, the contours of the volume fraction of circular tube is shown in Figs. 12d–f corresponding to the liquid spray density (Γ) of 0.04, 0.06 and 0.08 kg/(m s), respectively. It is clearly exhibited in these figures that the thickness of liquid film gradually increases with the increase in the spray density around the tube surface. Due to the advantage in the profile of the curvature with gravity force lead to increased acceleration of liquid film with reduced film thickness as pointed out by Luo et al. [7] for the drop-shaped and oval-shaped tubes.

It is observed from Fig. 13 that the thickness of liquid film varies from maximum at the impingement region to the highest value near the bottom of the tube with thinnest value at the mid region of the tube somewhere near the 90° angle based on the experimental and numerical studies carried out by Qi et al. [11]. In the present study, a CFD model is developed in the fluent software and simulation is carried out using the same operating parameters as followed by Qi et al. [11] in their studies. The results obtained from the CFD model is compared with the outputs of Qi et al. [11] and found relatively a good agreement in the range of 8%–16%. The simulation results of the film thickness from Qi et al. [11] and present study follows almost similar pattern along the curvature of the tube length as indicated in Fig. 13. But the thickness of the liquid film in the experimental study is found to be higher in the bottom of the tube as indicated in Fig. 13 compared with the CFD results. According to the present study, this difference could be due to the fact that no steam is supplied in the simulation model as done in the experimental study where the temperature of the wall of the tube would be fluctuating and also the condensation of the steam inside the tube disturbs the heat transfer mechanism that influences the physical properties of the liquid film at the bottom of tube. Hence the thickness is found to be lower in the CFD model compared with the experimental studies. Effect of spray density (Γ) on film thickness (mm) average around the tube surface for elliptical and circular tube at wall temp T_{wall} = 71.2°C, and T_{sat} = 70°C is indicated in Fig. 14. It is observed that increase of spray density leads to increase in the film thickness value on the tube surface. The result of Qi et al. [11] for both elliptical and circular tube of film thickness is compared with the results of the simulation model of the present study. A reasonably good agreement with a deviation of around 8%–16% and 10%–20% is observed between the present study and results of Qi et al. [11] corresponding to the elliptical and circular tube, respectively. It is also observed from the results of Qi et al. [11] that film thickness on the outer walls of elliptical is almost 10%–20% thinner than the

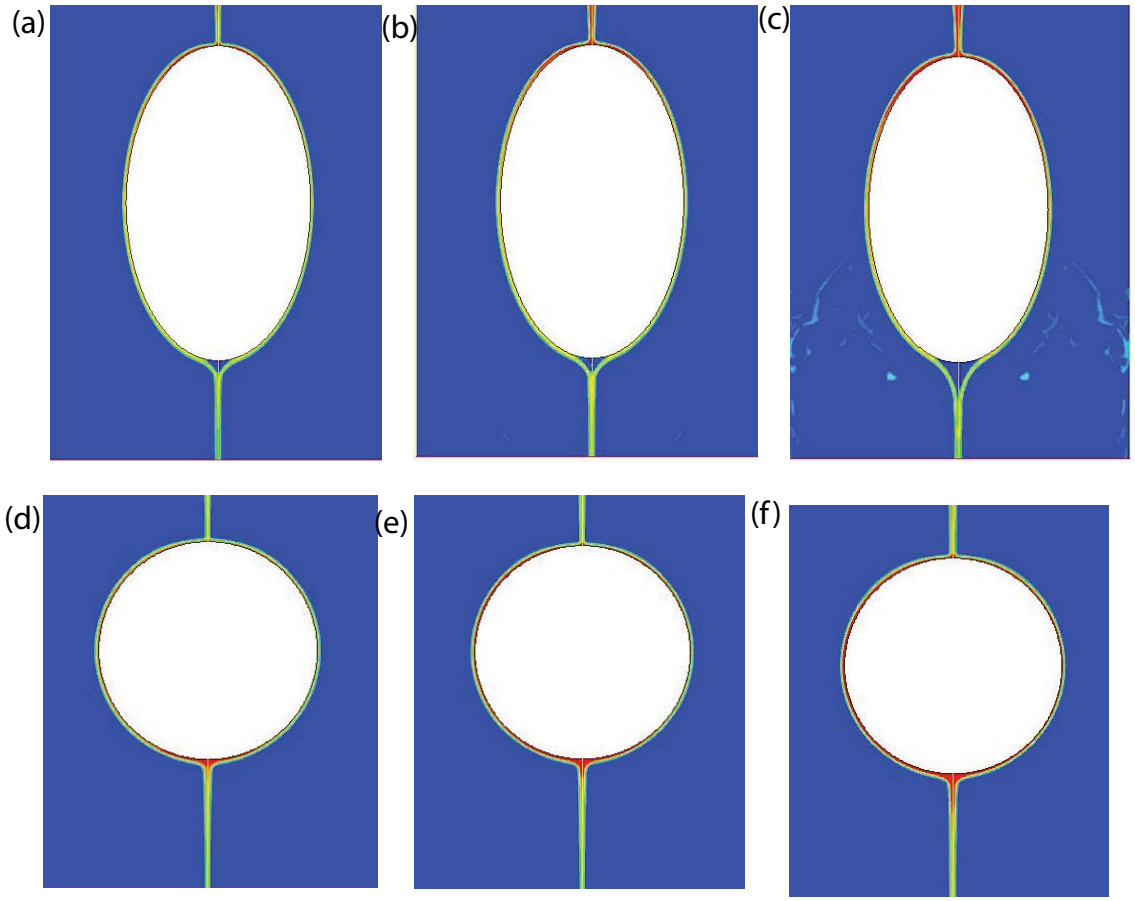

Fig. 12. Contours of volume fraction on elliptical tube and cylindrical tube for different spray density Γ (a) Γ = 0.04 kg/(m s), (b) Γ = 0.06 kg/(m s), (c) Γ = 0.08 kg/(m s), (d) Γ = 0.04 kg/(m s), (e) Γ = 0.06 kg/(m s), and (f) Γ = 0.08 kg/(m s).

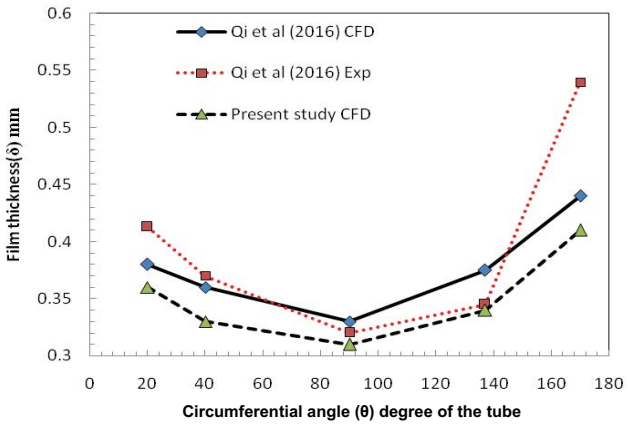

Fig. 13. Variation of film thickness (mm) around the circumferential position of tubes for elliptical tube at wall temperature T_{wall} = 71.2°C, Γ = 0.15 kg/(m s), T_{sat} = 70°C.

circular tubes, where as the present CFD study indicated that the film thickness of the elliptical tube is thinner by 8%–18% than the circular tubes. The thinnest film thickness for the elliptical tube is appearing between 90° and 110° angle and it varies with respect to the liquid spray density.

5.4. Effect of ellipticity on the HTC and liquid film thickness for varying spray density

Effect of ellipticity on the HTC and liquid film thickness is studied by carrying out CFD studies for different spray density and resultant values are compared and validated with the results of Qi et al. [11] as indicated in Fig. 15 for the film HTC and in Fig. 16 for liquid film thickness. Simulations have been done for two different ellipticity of tubes such as E = 1 and 1.5 in order to find out its influence on HTC and liquid film thickness values under varying feed water spray density. It is observed from Fig. 15 that with an increase in the spray density, the HTC values for the ellipticity of the tubes increases. It is also noticed that under the same operating conditions, the ellipticity of the tube with E = 1.5 exhibits better HTC than the tube with E = 1 for both Qi et al. [11] and present study. This could be due to the fact that increase of the ellipticity, that is, the ratio of major or vertical axis to the minor or horizontal axis of the elliptical tube absolutely resulted in the increase of perimeter area for the heat transfer which certainly promotes good driving force on the liquid film with large flow area. It is also observed from Fig. 16 that increase in the spray density of liquid film resulted in the increase of the liquid film thickness and increase of ellipticity lead to the decrease of the film thickness. The thickness of the liquid film for

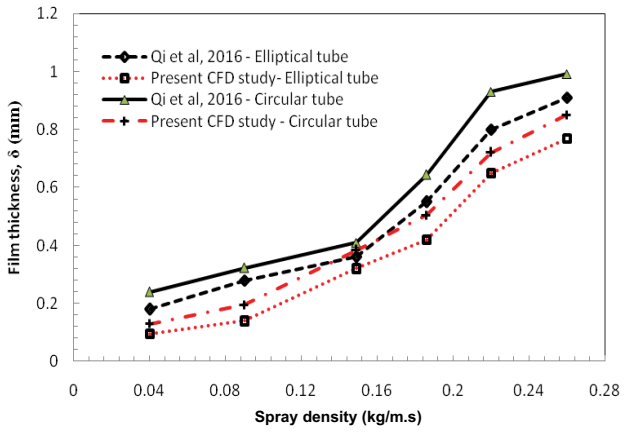

Fig. 14. Effect of spray density (Γ) on δ (mm) around the circumferential position of tubes for elliptical and circular tube at wall temperature T_{wall} = 71.2°C and T_{sat} = 70°C.

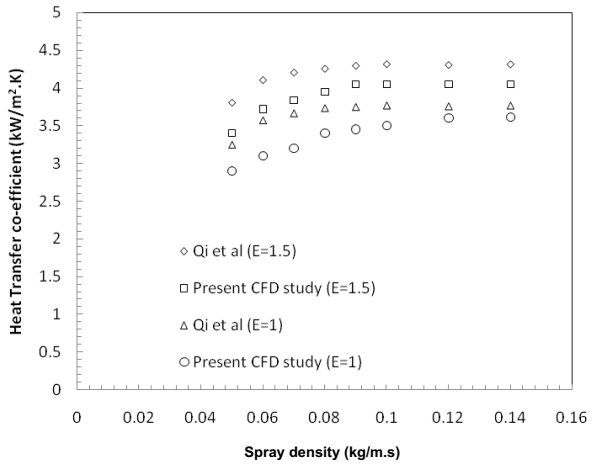

Fig. 15. Effect of ellipticity (*E*) on heat transfer co-efficient (kW/m^2 K) for varying spray density (Γ) (kg/(m s)) for elliptical tube at wall temperature T_{wall} = 71.2°C and T_{sat} = 70°C.

E = 1.5 is thinner compared with the *E* = 1 and this could be due to the fact that increased driving force acting on the liquid film resulted in the increased liquid film velocity, which in turn resulted in the decreased liquid film thickness and improved heat transfer rate. A good agreement of around 8%–11% and 10%–12% is observed between present study and results of Qi et al. [11] corresponding to the ellipticity of *E* = 1 and 1.5, respectively, for HTC as indicated in Fig. 15. It is also observed from Fig. 15 for the present CFD study that ellipticity of the tube *E* = 1.5 exhibits 10%–20% higher HTC than the tube with *E* = 1. Similarly, it is also observed from Fig. 16 that liquid film thickness of elliptical tube, *E* = 1.5 is almost 10%–15% thinner than the tube with *E* = 1.

6. Conclusions

CFD analysis was carried out using fluent software for validating the HTC, film thickness and commencement of fully developed region for both elliptical and circular tubes with experimental results and empirical correlations

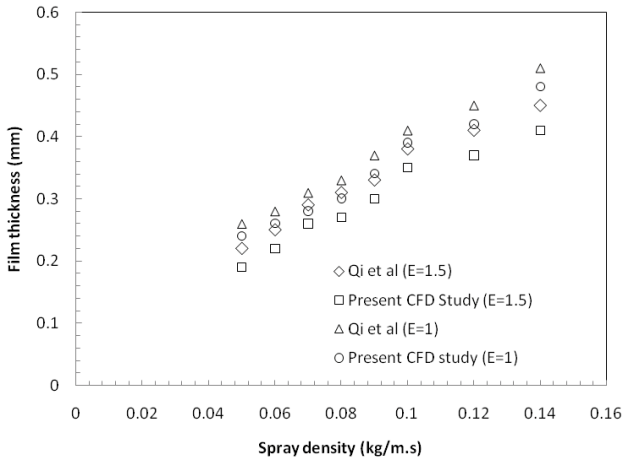

Fig. 16. Effect of ellipticity (*E*) on liquid film thickness (δ; mm) for varying spray density (Γ) (kg/(m s)) for elliptical tube at wall temperature T_{wall} = 71.2°C and T_{sat} = 70°C.

available in the literature by varying the liquid load. Similarly, the ellipticity of the tube and its effect on the HTC and film thickness was also validated and analysed with experimental data available in the literature. It was observed from CFD studies that elliptical tube improves HTC of falling film evaporation by 24%–26% (avg) compared with the circular tube for same operating conditions. It was noted that the elliptical tube reduces liquid film thickness on the outer surface by 8%–18% than the circular tube. Increase of the shape factor (*E*) from 1 to 1.5 enhances the HTC by 10%–20% and decreases liquid film thickness by 10%–15%. A low value of liquid film thickness was appeared between 90° and 110° angle on the tube circumference for elliptical tube. Finally, the novelty in predicting the commencement of fully developed region using the contours of the mass transfer rate from the simulation model is proved and validated with theory and mathematical model available in the literature.

Acknowledgement

The authors are highly thankful to Department of Science and Technology, Govt. of India (Grant Ref. No. DST/TMD/SERI/HUB/I(C)) for the financial support provided to Anna University, Chennai, India through ISEHC and Indian Institute of Technology Madras, Chennai for the successful completion of the present work.

Symbols

A	—	Heat transfer area of the tubes, m^2
C	—	Constant for tube diameter
Cp_l	—	Specific heat capacity of water, kJ/kg K
d	—	Tube diameter, m
g	—	Acceleration due to gravity, m/s^2
h	—	Heat transfer co-efficient, W/m^2 K
h_{fg}	—	Latent heat of evaporation, W/m^2 K
h_o	—	Film heat transfer co-efficient, W/m^2 K
k_l	—	Thermal conductivity of liquid, W/m K

L — Tube length, m
m_{in} — Mass flow rate of feed water, kg/s
m_v — Mass flow rate of vapour, kg/s
OD — Outer diameter
Pr — Prandtl number
q_f — Film heat transfer, W/m^2
q_w — Wall heat transfer, W/m^2
R — Radius of the tube
Re — Reynolds number
Ti — Feed intake temperature, °C
To — Brine discharge temperature, °C
T_s — Saturation temperature, °C
T_{static} — Static temperature, °C
T_w — Wall temperature, °C

Greek

Γ — Liquid spray density, kg/m s
μ_l — Dynamic viscosity, N-s/m^2
ρ_f — Density of fluid, kg/m^3
ρ_g — Density of gas, kg/m^3
ν_l — Kinematic viscosity, m^2/s
α_L — Thermal diffusivity, m^2/s
θ — Circumferential angle of tube, °

References

[1] D. Balaji, R. Velraj, M.V. Ramana Murthy, A review of the role of passive techniques on heat transfer enhancement of horizontal tube falling film and flooded evaporators, J. Enhanced Heat Transfer, 25 (2018) 239–282.
[2] K.R. Chun, R.A. Seban, Heat transfer to evaporating liquid films, ASME J. Heat Transfer, 93 (1971) 391–396.
[3] X.Hu, A.M. Jacobi, The intertube falling film. Part 2. Mode effects on the sensible heat transfer to a falling liquid film, J. Heat Transfer, 118 (1996) 626–633.
[4] S. Shen, X. Mu, G. Liang, X. Liu, Experimental investigation on heat transfer in horizontal tube falling film evaporator, Desal. Water Treat., 56 (2014) 1–7.
[5] F. Tahir, A. Mabrouk, M. Koc, Review on CFD analysis of horizontal falling film evaporators in multi effect desalination plants, Desal. Water Treat., 166 (2019) 296–320.
[6] E.N. Ganic, M.N. Roppo, An experimental study of falling liquid film breakdown on a horizontal cylinder during heat transfer, J. Heat Transfer, 102 (1980) 342–346.
[7] L. Luo, G. Zhang, J. Pan, M. Tian, Flow and heat transfer characteristics of falling water film on horizontal circular and non-circular cylinders, J. Hydrodyn., 25 (2013) 404–414.
[8] A. Hasan, K. Siren, Performance investigation of plain and finned tube evaporatively cooled heat exchangers, Appl. Therm. Eng., 23 (2003) 325–340.
[9] L. Chen, Z.Y. Chen, Falling film boiling heat transfer on horizontal elliptical tube, Chem. Eng. (China), 8 (1990) 35–40.
[10] A.E. Javad, M. Mahnaz, Entropy generation of forced convection film condensation on a horizontal elliptical tube, C.R. Mec., 340 (2012) 543–551.
[11] C.-h. Qi, H.-J. Feng, H.-q. Lv, C. Miao, Numerical and experimental research on the heat transfer of seawater desalination with liquid film outside elliptical tube, Int. J. Heat Mass Transfer, 93 (2016) 207–216.
[12] S. Sideman, D. Moalem, R. Semiat, Theoretical analysis of horizontal condenser-evaporator conduits for various cross sections, Desalination, 17 (1975) 167–192.
[13] Y.-T. Lee, S. Hong, C. Dang, L.-H. Chien, L.-W. Chang, A.-S. Yang, Heat transfer characteristics of obliquely dispensed evaporating falling films on an elliptical tube, Int. J. Heat Mass Transfer, 132 (2019) 238–248.
[14] Y.-T. Lee, S. Hong, C. Dang, L.-H. Chien, L.-W. Chang, A.-S. Yang, Effect of counter current air flow on film dispersion and heat transfer of evaporative falling film over a horizontal elliptical tube, Int. J. Heat Mass Transfer, 141 (2019) 964–973.
[15] L. Pu, Q. Li, X. Shao, L. Ding, Y. Li, Effects of tube shape on flow and heat transfer characteristics in falling film evaporation, Appl. Therm. Eng., 148 (2019) 412–419.
[16] M.C. Chyu, A.E. Bergles, An analytical and experimental study of falling film evaporation on a horizontal tube, J. Heat Transfer, 109 (1987) 983–990.
[17] D. Balaji, R. Velraj, M.V. Ramana Murthy, Numerical investigation on the effect of tube geometry and feeder height on the heat transformer performance of horizontal tube falling film evaporation, J. Heat Transfer, 141 (2019) 111502–111518.
[18] ANSYS Fluent Software Version 14.0.
[19] R. Bruce, S. Pascali, C. Vendramini, B. Baudouy, Implementation of the thermodynamic and phase transition equations of super fluid helium in CFD software, IOP Conf. Ser., 101 (2015) 012166.
[20] C.W. Hirt, B.D. Nichols, Volume of fluid (VOF) method for the dynamics of free boundaries, J. Comput. Phys., 39 (1981) 201–225.
[21] J.U. Brackbill, D.B. Kathe, C. Zemach, A continuum method for modelling surface tension, J. Comput. Phys., 100 (1992) 335–354.
[22] R. Sharma, Sushanta K. Mitra, Performance model for a horizontal tube falling film evaporator, Int. J. Green Energy, 2 (2005) 109–127.